LOW-EMITTANCE, LOW-CHARGE OPTIMIZATION OF THE ARGONNE WAKEFIELD ACCELERATOR FOR THE NANOPATTERNED MICROBUNCHING EXPERIMENT*

R. Margraf-O'Neal†, A. Ody, J. Power, Argonne National Laboratory, Lemont, United States
J. Maxson, Cornell University, Ithaca, United States
R. Ryne, Lawrence Berkeley National Laboratory, Berkeley, United States
H. Xu, N. Yampolsky, Los Alamos National Laboratory, Los Alamos, United States
G. Ha, B. N. Temizel Ozdemir, Northern Illinois University, DeKalb, United States
A. Halavanau, N. Majernik, SLAC National Accelerator Laboratory, Menlo Park, United States
G. Andonian, J. Phillips, J. Rosenzweig
University of California, Los Angeles, Los Angeles, United States
D. Abell, University of Maryland, College Park, College Park, United States

Abstract

Low-emittance microbunched electron beams are a key ingredient in free-electron lasers (FELs), facilitating gain and coherence in radiation production. It has been proposed, such as by the Compact X-ray FEL (CXFEL) group at Arizona State University, that nano-scale microbunching could be produced by rotating transverse beamlets into the longitudinal plane. Such a technique could make short-wavelength FELs much more compact, reducing cost. Thus, a collaboration has been formed to test this principle using the emittance exchange (EEX) beamline of the Argonne Wakefield Accelerator (AWA). This experiment will take micro-scale transverse modulations on a TEM grid and produce mico-to-nano scale microbunches. Performing this with AWA's 40 MeV electron beam will require low normalized emittance ($\approx$50 nm $\cdot$ rad), and low charge ($\approx$1pC) electron bunches that are not commonly produced at AWA. These proceedings will detail our work to produce and characterize this low emittance in the AWA beamline.

INTRODUCTION

The nanopatterned microbunching experiment [1, 2], to take place in 2027-2028, is sketched in Fig. 1. 44 MeV electrons are scattered by a 12.5 µm TEM grid, creating transverse beamlets that are then demagnified with beamline of five quadrupoles [3] to 3 µm, and converted through emittance exchange to 800 nm microbunching.

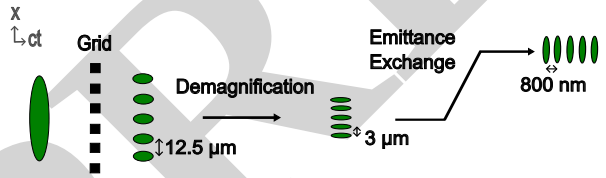

Figure 1: Nanopatterned microbunching experiment.

The nanopatterned microbunching experiment has several requirements on the AWA facility that are outside of its normal operating range. AWA is tuneable within a large charge range (1 pC - 400 nC), but optimized for high charge (100s of nC) bunch trains to drive structure wakefield acceleration [4, 5]. However, to mitigate collective effects, the nanopatterned microbunching experiment must operate at low charge (2-6 pC incident on the TEM grid). Low normalized emittance (50 nm $\cdot$ rad) must be achieved at this charge to preserve the closely spaced transverse beamlets. Our previous measurements in this range, however, found micron-scale normalized emittance at 1 pC [2]. This proceedings will document our progress to push this emittance lower in our development of this low-charge, low-emittance mode for the nanopatterned microbunching experiment.

Two beamtimes, in July 2025 and April 2026, are described in this proceedings. Between these two beamtimes, the AWA gun was replaced and upgraded to a symmetrized design, and the gun solenoids and Ce_2Te photocathode were also replaced. Thus, this proceedings also documents how the AWA gun upgrade changed our measured emittance.

METHODS

High-Resolution Transverse Diagnostics

We installed a Blackfly camera (BFLY-PGE-23S6M-C) with a Nikon AF FX 200 mm f/4D IF-ED Lens and 381 mm (for knife scan) or 62 mm (for quad scan) extension tube. This was focused on a 100 µm thick YAG:Ce screen after a 45° mirror reflection. The light path distance from the YAG to the vacuum chamber window was 165 mm, and the working distance from the end of the camera lens to the YAG was 178 mm or 210 mm respectively.

This set-up resulted in a 1.30 µm and 3.60 µm pixel size. Using a US Air Force target in the installed system, the camera resolution was measured to be 6.2 µm and 7.0 µm for each configuration.

Studying this system [2, 6] indicated that our high-resolution imaging system, with its thick, 100 µm YAG:Ce screen, can only resolve electron beams down to σ = 40-50 µm. In future upgrades, we plan to replace the

* This work is supported by the U. S. Department of Energy, under contract No. DE-AC02-06CH11357.
† rachel4iam@gmail.com

100 µm thick YAG:Ce with a 20 µm thick YAG:Ce for improved resolution.

Charge Measurement

AWA's primary charge detectors are an integrated current transformers (ICTs), which are sensitive down to 20 pC. AWA also has a beam position monitor (BPM). Summing the signal from the four channels of the BPM provides a more sensitive charge diagnostic. Example waveforms are shown in Figs. 2A and 3A. When calibrated against the ICT signal, as shown in Figs. 2B and 3B, the BPM can detect charges down to ≈1 pC. The ICT used for calibration here is located after the first linac module, and the BPM is located after the beam has reached 44 MeV, right before our imaging diagnostic.

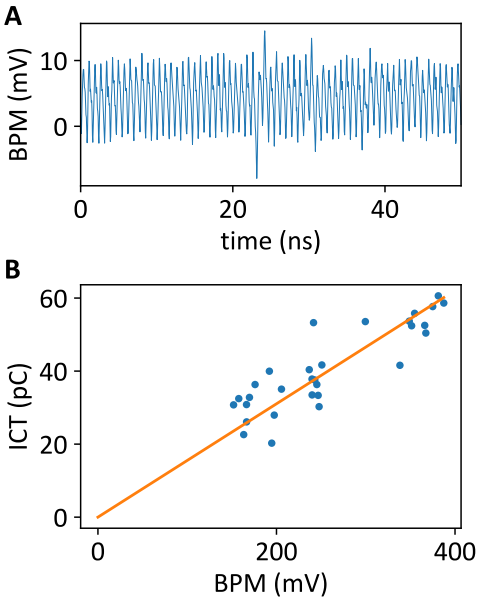

Figure 2: Low charge detection with a BPM, July 2025. A) Time-dependent trace for a 3.5 pC bunch, showing a signal peak. B) Calibration of the BPM peak height against AWA's ICT (slope = 0.155 mV/pC).

Quadrupole Emittance Measurements

Our first emittance measurement technique was a quadrupole scan. A 44 MeV electron beam was sent through a quadrupole to our imaging system 5.54 m downstream. The quadrupole strength was scanned, and the beam size was measured on the downstream screen as depicted in Figs. 4 and 5. The matching solenoid strength in the electron gun was varied to search for the solenoid focusing which minimized the emittance. The fitted beam size plots were used to calculate emittance based on a thick quadrupole matrix transport.

Knife-Edge Scan Emittance Measurements

Our second emittance measurement technique, which has only been analyzed for the July 2025 measurement thus far, was a knife-edge scan. The edge of a 2 mm wide stainless

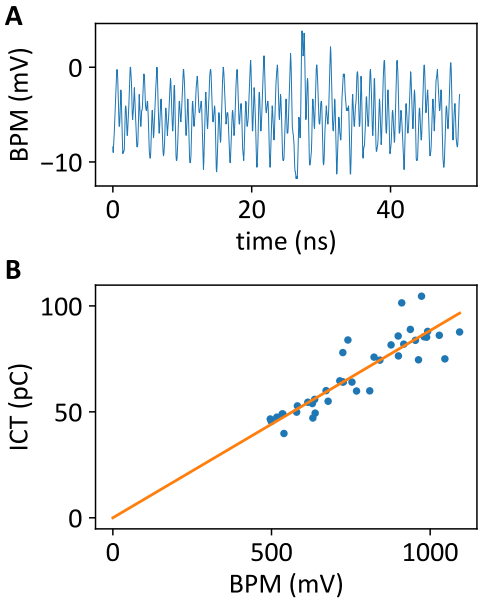

Figure 3: Low charge detection with a BPM, April 2026. A) Time-dependent trace for a 1.4 pC bunch, showing a signal peak. B) Calibration of the BPM peak height against AWA's ICT (slope = 0.088 mV/pC).

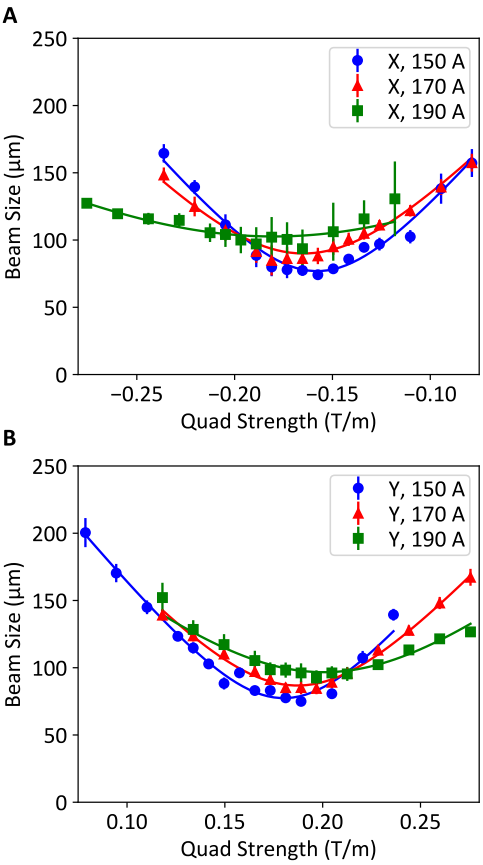

Figure 4: July 2025 quadrupole scan for 3 different currents of the gun matching solenoid in A) X and B) Y. Error bars give the standard error of the mean.

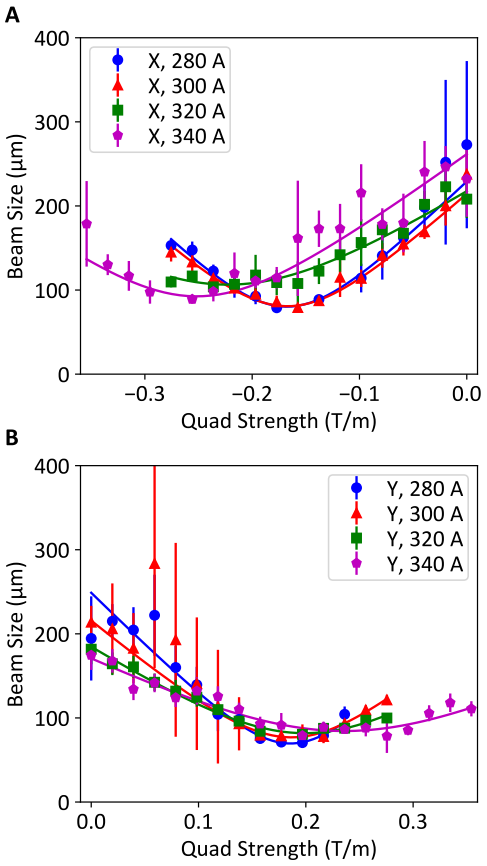

Figure 5: April 2026 quadrupole scan for 4 different currents of the upgraded gun matching solenoid in A) X and B) Y. Error bars give the standard error of the mean.

steel slit was used as a knife-edge and scanned through the beam. The beam was then collected by our imaging system 2.87 m downstream of the knife-edge.

The resultant data was analyzed following a 1D version of a method described by Ji [7]. The unblocked beam projected onto the y-axis was first fit with a Gaussian to find the beam size and center at the detector, y_1 and σ_{y1}. Then, with y_1 and σ_{y1} fixed, the partially blocked beam projected onto the y-axis ($\rho_y(y)$) was fit using Equations 1-2, where Q_0 is an arbitrary constant:

$$\rho_y(y) = \frac{1}{2}\rho_0(y)\left[1 + erf\left(\frac{y - y_1 - M_y y_k}{\sqrt{2}\sigma_k}\right)\right], \quad (1)$$

$$\rho_0(y) = \frac{Q_0}{\sigma_{y1}\sqrt{2\pi}} e^{\frac{-(y-y_1)^2}{2\sigma_{y1}^2}}. \quad (2)$$

This fit, as shown in Fig. 6, gives the blur on the knife edge σ_k, and the product of the magnification and the knife-edge transverse scan step, $M_y y_k$. By comparing these fits across the region of this scan that could successfully fit, we found the M_y and σ_k as shown in Figs. 7A-B.

To determine the beam size and center at at the knife-edge location, y_0 and σ_{y0}, we then fit the normalized intensity of the screen through the knife-edge scan, Q, using:

$$Q = \frac{Q_0}{2}\left[1 + erf\left(\frac{y_k - y_0}{\sqrt{2}\sigma_{y0}}\right)\right] \quad (3)$$

and as shown in in Fig. 7C.

Normalized emittance was then found using:

$$\epsilon_{N,y} = \frac{\gamma\sigma_{y0}\sigma_k}{LM_y}, \quad (4)$$

where γ is the relativistic γ and L is the distance between the knife-edge and the screen.

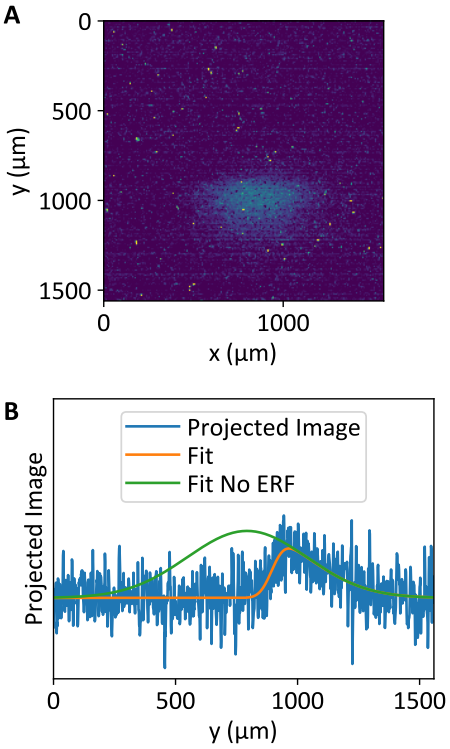

Figure 6: Fitting a sample knife scan image. A) Sample image of a mostly-blocked beam, B) Y-projection of this image. The orange trace gives the fit from Equation 1, and the orange trace gives a fit for a Gaussian of the unblocked beam size, $\sigma_{y1} = (245 \pm 8)$ μm.

RESULTS

The emittances measured by the quadrupole scans and knife-edge scan are given in Table 1.

By scanning the strength of the gun matching solenoid, the lowest normalized emittance we were able to achieve was $\epsilon_{x,N} = (220 \pm 20)$ nm · rad, $\epsilon_{x,N} = (330 \pm 20)$ nm · rad before the gun upgrade, and $\epsilon_{y,N} = (220 \pm 20)$ nm · rad, $\epsilon_{x,N} = (250 \pm 20)$ nm · rad, $\epsilon_{y,N} = (150 \pm 20)$ nm · rad after the gun upgrade.

This improvement of emittance may be due to improvements in the symmetrized gun field, a more optimal setting of the gun matching solenoid, or less space charge effects from the lower charge (1 pC) of the April 2026 experiment, versus the 3 pC beam in the July 2025 experiment.

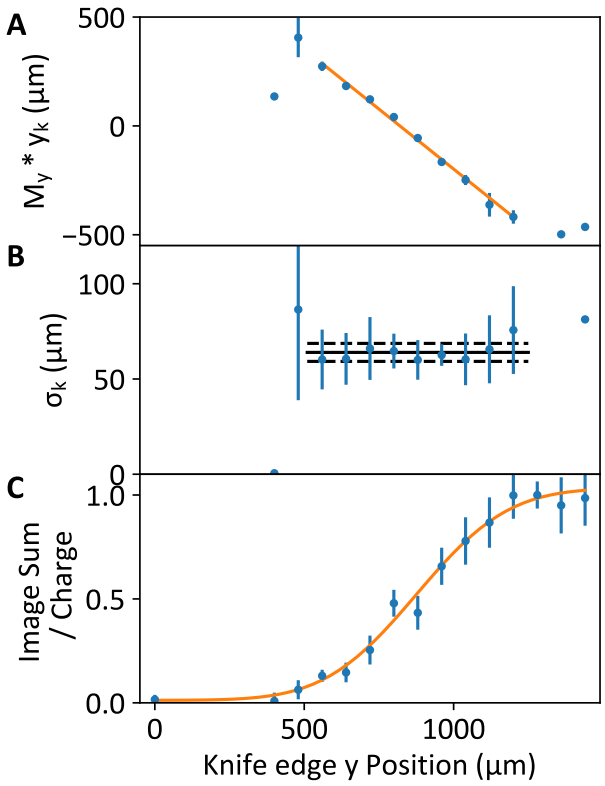

Figure 7: Knife-edge scan parameter fitting. A) The product of M_y and y_k was fit as a single parameter at each scan point. The magnification, $M_y = 1.1$, was found from the slope of these fitted parameters in the scan region where the beam can be well fit. B) $\sigma_k = (64 \pm 5)$ μm was found from the mean σ_k in the region of the scan where σ_k can be well fit. The solid line gives the mean value, and the dashed line gives the standard error of the mean. C) The plot of normalized image sum from which $\sigma_{y0} = (240 \pm 20)$ μm is fit. Error bars give the standard error of the mean.

Since the gun matching solenoid was replaced between these two beam times, the solenoid current is not comparable between the two beam times, and we will have to examine the solenoid field maps to determine if the setting used in the more recent beam time produces a stronger or weaker field than the previous beam time.

The photocathode laser spot size was also slightly larger in the April experiment, measuring full widths of $FW_x = 340\,\mu$m, $FW_y = 360\,\mu$m in July 2025, and $FW_x = 440\,\mu$m, $FW_y = 470\,\mu$m in April 2026. Ordinarily, we would expect that a smaller laser spot size would produce a smaller emittance. Thus, we do not expect that the small change in the laser spot size at the photocathode had a large effect on the emittance improvement.

DISCUSSION AND FUTURE WORK

Our best measured normalized emittance of $\epsilon_{x,N} = (250 \pm 20)$ nm · rad, $\epsilon_{y,N} = (150 \pm 20)$ nm · rad is still a factor of 5 in X and 3 in Y larger than our target of $\epsilon_N = 50$nm · rad. The results from the April 2026 measurement show emittance decreasing with increased matching solenoid strength, so we may be able to further decrease the emittance with a stronger solenoid field. Additionally, we can further improve our laser system to reduce the smallest achievable spot size on the photocathode. With additional improvements, we are steadily getting closer to the emittance needed to run the nanopatterned microbunching experiment in 2027-2028.

Table 1: Measurements of electron bunch charge and normalized emittance. The AWA gun was upgraded to a symmetrized version and the gun solenoids were replaced between the two beam times.

July 2025 Knife-Edge Scan			
Solenoid Current (A)	Charge (pC)		$\epsilon_{y,N}$ (nm·rad)
150	3		430 ± 60
July 2025 Quadrupole Scan			
Solenoid Current (A)	Charge (pC)	$\epsilon_{x,N}$ (nm·rad)	$\epsilon_{y,N}$ (nm·rad)
150	3	370 ± 20	390 ± 20
170	3	390 ± 20	400 ± 20
190	2.8, 2.7	220 ± 20	330 ± 20
April 2026 Quadrupole Scan			
Solenoid Current (A)	Charge (pC)	$\epsilon_{x,N}$ (nm·rad)	$\epsilon_{y,N}$ (nm·rad)
280	1.2	280 ± 20	250 ± 20
300	1.2, 1.1	270 ± 10	230 ± 20
320	0.9	250 ± 20	190 ± 20
340	0.8	250 ± 20	150 ± 20

REFERENCES

[1] G. Ha *et al.*, "Coherent radiation from initially modulated beams using emittance exchange at the Argonne Wakefield Accelerator", *Nucl. Instrum. Methods Phys. Res. A*, vol. 1075, p. 170387, Jun. 2025. doi:10.1016/j.nima.2025.170387

[2] R. Margraf-O'Neal *et al.*, "Low-charge, high-resolution beamline preparation for the nanopatterned microbunching experiment at argonne wakefield accelerator", in *Proc. NAPAC2025*, Sacramento, CA, USA, pp. 173–176, Aug. 2025. doi:10.18429/JACoW-NAPAC2025-MOP055

[3] B. T. Ozdemir and G. Ha, "Start-to-end simulations of nanometer-emittance beam transport through an emittance exchange beamline", in *Proc. NAPAC2025*, Sacramento, CA, USA, pp. 588–591, Aug. 2025. doi:10.18429/JACoW-NAPAC2025-TUP092

[4] L. Zheng *et al.*, "Rapid thermal emittance and quantum efficiency mapping of a cesium telluride cathode in an rf photoinjector using multiple laser beamlets", *Phys. Rev. Accel. Beams*, vol. 23, no. 5, p. 052801, May 2020. doi:10.1103/PhysRevAccelBeams.23.052801

[5] J. G. Power, M. E. Conde, W. Gai, Z. Li, and D. Mihalcea, "Upgrade of the Drive LINAC for the AWA Facility Dielectric Two-Beam Accelerator", pp. 4310–4312. http://accelconf.web.cern.ch/IPAC10/papers/THPD016.pdf

[6] R. Margraf-O'Neal *et al.*, "Selection of transverse diagnostics to measure few-micron beam modulations in the nanopatterned microbunching experiment", presented at IPAC'26, Deauville, France, May 2026, paper MOP6355, this conference.

[7] F. Ji, J. G. Navarro, P. Musumeci, D. Durham, A. Minor, and D. Filippetto, "Knife-edge based measurement of the 4D transverse phase space of electron beams with picometer-scale emittance", *Phys. Rev. Accel. Beamss*, vol. 22, no. 8, p. 082801, Aug. 2019. doi:10.1103/PhysRevAccelBeams.22.082801